



Groundwater flow with energy transport and water–ice phase change: Numerical simulations, benchmarks, and application to freezing in peat bogs

Jeffrey M. McKenzie^{a,*}, Clifford I. Voss^b, Donald I. Siegel^c

^a Department of Earth and Planetary Sciences, McGill University, 3450 University Avenue, Montreal, QC, Canada H3A 2A7

^b U.S. Geological Survey, 431 National Center, Reston, VA 20192, USA

^c Department of Earth Sciences, 204 Heroy Geology Laboratory, Syracuse University, Syracuse, NY 13224, USA

Received 3 June 2005; received in revised form 19 August 2006; accepted 21 August 2006

Abstract

In northern peatlands, subsurface ice formation is an important process that can control heat transport, groundwater flow, and biological activity. Temperature was measured over one and a half years in a vertical profile in the Red Lake Bog, Minnesota. To successfully simulate the transport of heat within the peat profile, the U.S. Geological Survey's SUTRA computer code was modified. The modified code simulates fully saturated, coupled porewater-energy transport, with freezing and melting porewater, and includes proportional heat capacity and thermal conductivity of water and ice, decreasing matrix permeability due to ice formation, and latent heat. The model is verified by correctly simulating the Lunardini analytical solution for ice formation in a porous medium with a mixed ice–water zone. The modified SUTRA model correctly simulates the temperature and ice distributions in the peat bog. Two possible benchmark problems for groundwater and energy transport with ice formation and melting are proposed that may be used by other researchers for code comparison.

© 2006 Elsevier Ltd. All rights reserved.

Keywords: Groundwater; Peat; Energy transport; Freezing; Cold regions; Benchmark; Modelling

1. Introduction

The freezing and thawing of subsurface water in regions experiencing subzero air temperatures can directly affect numerous hydrogeological, and biological processes, including the thermal regime, groundwater flow patterns, groundwater recharge, and subterranean biological activity [1–3]. Further, given the sensitivity of arctic regions to climatic changes [e.g. [4,5]], understanding the processes that control the formation and extent of ice is important.

The interaction of near-surface water and ice with the regional groundwater regime also partly controls where and the rate at which subsurface ice forms. For example,

in northern peatlands the thermal regime is controlled both by seasonal temperature fluctuations and the advection of deeper, warmer water [6,7]. Ice in upper soils in these regions can affect groundwater flow in complex feedback mechanisms. For example, by forming a temporary confining zone, ice can both diminish upward discharge of groundwater and potential recharge of aquifers by precipitation [8,9]. The melting ice may itself be controlled to some extent by convection of heat [10]. Ice also affects how contaminants may be transported in the subsurface [e.g. [11]]. Thermal models in northern climates have been used to reconstruct and estimate climate change. For these reasons, it is important to establish models that simulate conduction, advection, and water-to-ice phase changes.

The transport of heat in the subsurface is controlled by conduction due to a temperature gradient [12] and can also

* Corresponding author. Tel.: +1 514 398 3833.

E-mail address: mckenzie@eps.mcgill.ca (J.M. McKenzie).

Nomenclature

Symbol Definition

γ_0^w	energy sources in the fluid
γ_0^s	energy sources in the solid grains
ε	porosity
ε_i	fractional volume of ice
ε_s	fractional volume of solid matrix
ε_w	fractional volume of liquid water
λ	thermal conductivity
λ_i	thermal conductivity of ice
λ_s	thermal conductivity of solid matrix
λ_w	thermal conductivity of liquid water
ρ	density of liquid water
ρ_i	density of ice
ρ_s	density of solid matrix
μ	viscosity of liquid water
Ω	impedance factor
B_T	residual saturation temperature (Eq. (7))
c_i	heat capacity of ice
c_s	heat capacity of solid matrix
c_w	heat capacity of water
C_a	apparent heat capacity
\underline{D}	dispersion tensor
\underline{I}	identity tensor
\underline{k}	permeability tensor
k_r	relative permeability
L_f	latent heat of formation
m	slope of linear freezing function
p	pressure
Q	ice content
Q_p	porewater inflow
S_i	saturation of ice
S_{op}	specified pressure storativity
S_w	saturation of liquid water
S_{wres}	residual saturation
t	time

T	temperature
T^*	temperature of the source fluid
T_{air}	air temperature
T_L	freezing point temperature (Eq. (9))
\underline{v}	average fluid velocity
w	fitting parameter for exponential freezing function

Lunardini solution

α_1	thermal diffusivity of fully frozen zone
α_3	thermal diffusivity of fully liquid zone
α_4	thermal diffusivity of ‘mushy’ zone
γ	solution parameter for Eqs. (27) and (28)
γ_d	dry unit density of soil solids
ξ_f	ratio of unfrozen water to soil solid mass for frozen zone
ξ_0	ratio of unfrozen water to soil solid mass for fully thawed zone
ψ	Solution parameter for Eqs. (27) and (28)
C_1	volumetric bulk heat capacity of frozen zone (Eq. (18))
C_3	volumetric bulk heat capacity of fully thawed zone (Eq. (19))
k_1	bulk thermal conductivities of the frozen zone (Eq. (20))
k_2	bulk thermal conductivity of fully thawed zone (Eq. (21))
T_1	temperature at distance x in fully frozen zone
T_2	temperature at distance x in ‘mushy’ zone
T_3	temperature at distance x in fully thawed zone
T_f	liquidus temperature
T_m	solidus temperature
T_0	initial condition temperature
T_s	boundary temperature
x	distance

be influenced by advection of flowing porewater [e.g. [13]]. Where there is seasonal or annual freezing of porewater in the subsurface, the formation and melting of ice will affect heat conduction because the bulk thermal properties of the soil change. Ice has a different heat capacity and thermal conductivity than liquid water and solid aquifer matrix [14]. The latent heat released as ice forms can be at least ten times greater than that released by heat capacity alone [15].

The advection of heat is also affected by the formation of ice. Porewater velocities decrease with ice formation [16] and the decrease in hydraulic conductivity in places may temporarily confine shallow groundwater flow systems. Finally, freezing and thawing of porewater may interact with groundwater flow systems and precipitation/snow melt at the land surface in complex feedback mechanisms [10].

Several numerical models incorporate freezing and thawing processes into porewater flow models. An early

model by Hwang et al. [17] simulated the interaction of surface structures on permafrost. Hansson et al. [18] simulated water and vapor flow with a 1-dimensional model based on the HYDRUS-1D model [19]. Ippisch [20] simulated water and vapor flow using a finite difference approach and found that for permafrost situations, the flow of water in near-freezing regimes is the most important control on ice extent. Mottaghy and Rath [21] used a finite difference model [22] for saturated porewater flow with ice formation to show the importance of latent heat in reconstructing paleoclimate using borehole temperature inversions. The STOMP model [23] was designed for the transport of organic contaminants in the subsurface and includes the freezing and thawing of porewater. The COUP [24] and SHAW [25] models are 1-dimensional simulators of heat, with freezing and thawing, and mass transfer. The TEMP/W [26] model, a numerical simulation of the freez-

ing and thawing of pore water where freezing is limited to a calculated freezing zone, is an add-on component for the geotechnical GEO-SLOPE modeling environment.

Models of heat transport in the subsurface for cold regions with ice formation must incorporate changes in thermal and hydraulic properties as a function of ice content. Presented herein is SUTRA-ICE, a numerical model that incorporates ice formation and melt as a modification to the SUTRA numerical solute, heat, and water transport code [27] for the case of fully saturated flow. SUTRA-ICE can simulate the phase transformation of porewater to ice over a range of subfreezing temperatures (without ice segregation or layering), along with the associated changes in heat capacity, thermal conductivity, relative permeability, density, and the latent heat of formation. The model presented here is fully 3-dimensional and is easily modified by the user. The SUTRA-ICE model is verified by comparing its results to a closed-form analytical solution for ice formation [28]. Two potential 2-dimensional benchmark problems are suggested that incorporate both flowing porewater and ice formation. Finally, the modified code is applied to evaluate the impact of ice formation on temporal changes of the thermal profile in a large peat bog.

2. Methods

2.1. Numerical model

The SUTRA computer code [27,29] is modified to incorporate freezing and thawing properties within the context of its energy transport model. The modifications are for intermediate and regional hydrogeologic spatial scales, and focus on the interaction of ice formation/melting with groundwater flows and temperature regimes in the subsurface that affects the location and temporal persistence of groundwater recharge and discharge areas. Pressure effects that cause mechanical changes, particularly pore-size increase and ice-lensing, are a different focus than the objectives of our research and model development. SUTRA allows modeling of variable density, mass transport of fluid, solute and/or energy transport under saturated and/or unsaturated conditions, and it solves the set of governing equations for thermal energy and fluid and chemical mass transport through a combination of finite element and finite difference approximations. SUTRA is very powerful because it can be configured to represent a wide range of hydrogeologic conditions, and new processes can be easily added by the user.

The code is modified by changing the spatial properties of the porous matrix that occur when temperatures at a specific model node or element are below the freezing point, 0 °C. These include the effects of ice on the thermal conductivity, heat capacity, permeability of the porous medium, and the latent heat of formation of ice. Values of thermal conductivity and heat capacity change as a function of ice content, and are based on volume-weighted averages through the soil profile as a first approximation

[15]. It is assumed that the ice is immobile, the medium is nondeformable, and freezing point depression due to solute concentrations is negligible.

2.2. Thermal properties

The bulk thermal conductivity, λ , including solid matrix, water and ice is calculated by a volumetric average approximation [15]:

$$\lambda = \varepsilon S_w \lambda_w + \varepsilon S_i \lambda_i + (1 - \varepsilon) \lambda_s \quad (1)$$

where ε is the porosity, S_w and S_i are the saturation of liquid water and ice, and λ_w , λ_s , and λ_i are the thermal conductivities of liquid water, the solid matrix, and ice, respectively. If there is no ice, then Eq. (1) simplifies to the original equation for thermal conductivity used in SUTRA, $\lambda = \varepsilon S_w \lambda_w + (1 - \varepsilon) \lambda_s$. The saturation of ice and water consists of their relative volumetric proportions within the pores. The SUTRA-ICE model presented herein assumes fully saturated conditions and therefore:

$$S_w + S_i = 1 \quad (2)$$

$$\frac{\partial S_w}{\partial T} = - \frac{\partial S_i}{\partial T} \quad (3)$$

where T is temperature. An apparent heat capacity, C_a , is used [18,30] that incorporates both the heat capacity of ice and the latent heat:

$$C_a = \varepsilon_w \rho c_w + \varepsilon_i \rho_i c_i + \varepsilon_s \rho_s c_s + \varepsilon \rho_i L_f \frac{\partial S_w}{\partial T} \quad (4)$$

where $\varepsilon_w = \varepsilon S_w$, $\varepsilon_i = \varepsilon (1 - S_w)$, and $\varepsilon_s = (1 - \varepsilon)$ are the liquid water, ice, and solid matrix fractional volumes respectively, ρ , ρ_i , and ρ_s are the densities of liquid water, ice and the solid matrix respectively, c_i , c_s , and c_w are the heat capacities of ice, solid matrix and water respectively, L_f is the latent heat of formation of ice, and $\varepsilon \rho_i \partial S_w / \partial T$ is the mass of water per volume porous medium that is produced by melting as T increases. Assuming fully saturated conditions, the apparent heat capacity is:

$$C_a = \varepsilon (S_w \rho c_w + S_i \rho_i c_i) + (1 - \varepsilon) \rho_s c_s - \varepsilon \rho_i L_f \frac{\partial S_i}{\partial T} \quad (5)$$

2.3. Soil freezing functions

In soils, porewater freezes over a range of temperatures below freezing [15]. As soil temperatures decrease below the freezing point for pure ice, there is a slight freezing point depression because of dissolved salts in the porewater. Once ice starts to form, ice does not immediately crystallize, but forms gradually. Capillary and absorptive forces are amplified as more water is converted to ice [15] because more of the remaining fluid exists in the form of thin films. Even when most of the soil water is frozen, a small amount of super-cooled, unfrozen soil water remains which is the residual saturation, S_{wres} . The residual unfrozen water consists of water molecules attached to grain surfaces and water that has a significantly decreased freezing point caused by

increased dissolved solids that are excluded by ice formation. The freezing function for water-saturated soils is similar in shape to the saturation function for unsaturated soils, but depends on temperature instead of pressure (Fig. 1).

There are numerous functions used to describe the freezing of a soil. Fig. 2 shows two commonly used functions (without hysteresis) and derivatives of them. The freezing

function should be smooth and easily differentiated, because the derivative $\partial S_i / \partial T$ is used to determine the apparent heat capacity in Eq. (5). The simplest freezing function is a linear function:

$$S_w = mT + 1 \quad \text{if } T > B_T$$

$$S_w = S_{wres} \quad \text{if } T < B_T \quad (6)$$

where m is the slope of the freezing function, and B_T is defined as the temperature at which the linear freezing function attains residual saturation, S_{wres} , defined as:

$$B_T = \frac{S_{wres} - 1}{m} \quad (7)$$

The derivative of the linear freezing function (Eq. (6)) is:

$$\frac{\partial S_w}{\partial T} = m \quad \text{if } T > B_T$$

$$\frac{\partial S_w}{\partial T} = 0 \quad \text{if } T < B_T \quad (8)$$

Another possible freezing function is an exponential function [31]:

$$S_w = (1 - S_{wres}) \exp \left[- \left(\frac{T - T_L}{w} \right)^2 \right] + S_{wres} \quad (9)$$

where T_L is the liquidus or freezing point, usually 0 °C, and w is a fitting parameter. The derivative of the exponential freezing function with respect to temperature is:

$$\frac{dS_w}{dT} = - (1 - S_{wres}) \frac{2(T - T_L)}{w^2} \exp \left[- \left(\frac{T - T_L}{w} \right)^2 \right] \quad (10)$$

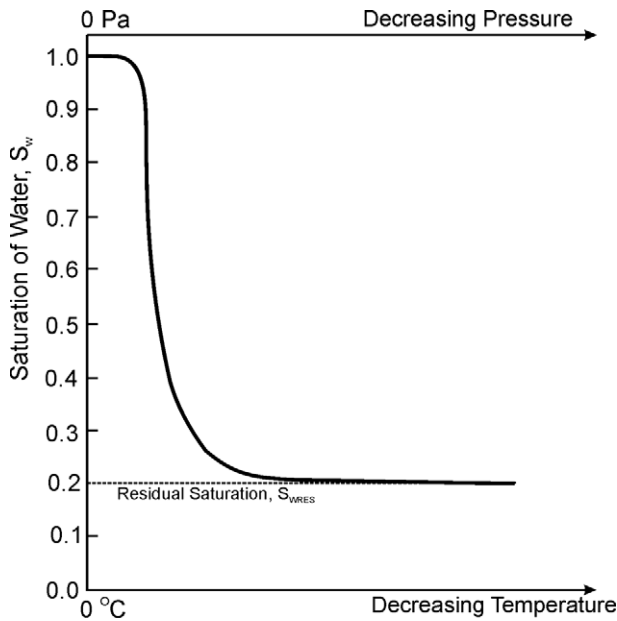


Fig. 1. Generalized plot showing the analogy between the soil characteristic function and soil freezing function for a given soil.

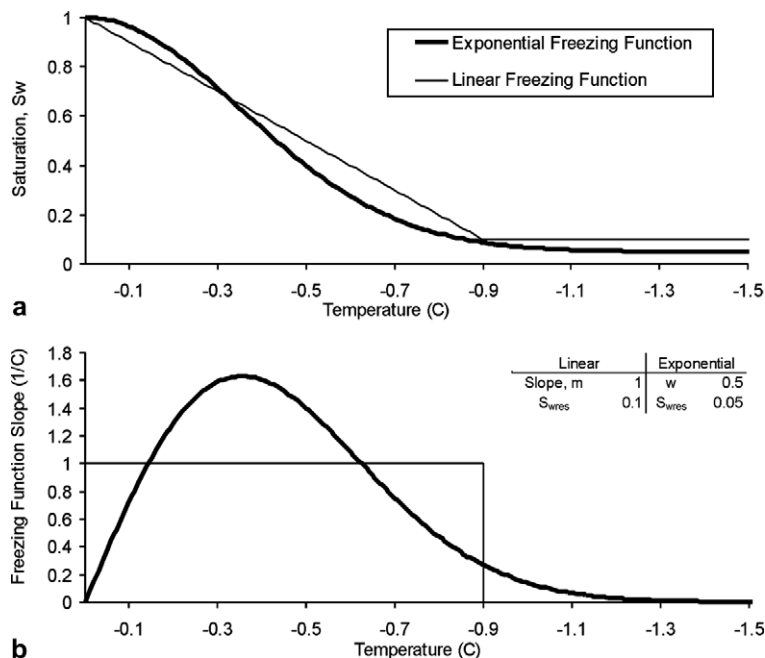


Fig. 2. (a) Examples of two possible freezing functions, the exponential and the linear, which can be used to describe the formation of ice with temperatures below 0 °C in soils, as described by Eqs. (6) and (9) and (b) The slopes of the functions in Fig. 2a. Inset Table: Parameters used for the two functions shown.

2.4. Permeability

Ice that forms in pore space will decrease the permeability as it clogs open pores and restricts the movement of water. To represent this decrease, a relative permeability, k_r , is used, where the effective permeability is the product of the fully saturated permeability and the relative permeability. The relative permeability is less than unity for ice saturations greater than zero. The relative permeability cannot equal zero, or the flow equation cannot be solved; however, a very small minimum value can be set.

The simplest function for changes in the relative permeability with ice formation is a linear decrease in k_r for temperatures between freezing and the temperature at which the residual saturation (B_T ; Eq. (7)) is reached. At this point, an arbitrary small minimum value (10^{-6}) of k_r is assigned:

$$k_r = \left(\frac{10^{-6} - 1}{B_T} \right) T + 1 \quad \text{if } T > B_T \quad (11)$$

$$k_r = 10^{-6} \quad \text{if } T < B_T$$

An impedance factor can also be used to calculate the relative permeability k_r [32]. Again, the minimum relative permeability is limited at 10^{-6} .

$$k_r = 10^{-\Omega Q} \quad \text{if } 10^{-\Omega Q} > 10^{-6} \quad (12)$$

$$k_r = 10^{-6} \quad \text{if } 10^{-\Omega Q} \leq 10^{-6}$$

where Ω is the empirically derived impedance factor, and Q is defined as the ice content, equal to εS_i . Hansson et al. [18] use a different definition of Q : the ratio of the ice content to the total (minus the residual) water content.

The direct measurement of the freezing function for a given soil is difficult, and limited data is available for most soil types [14,33]. Koopmans and Miller [34] empirically found that for a given soil, the characteristic shape of the saturation function (for unsaturated soils) is the same as the shape of the freezing function for fully saturated soils (Fig. 1). The relationship between the two similar functions depends only on the ratio of interfacial tensions between the air–water and water–ice interfaces [35] and the water–air and ice–water pressures calculated using the Clapeyron equation [36]. If the relationship between the two functions can be calculated, one can employ a known (e.g. laboratory-measured) unsaturated function for a soil as the soil's freezing function. For example, Grant [37] provides a method for using the unsaturated van Genuchten function [38] for calculating the freezing function and relative permeability due to ice formation. However, this alternative approach is not used in the examples discussed herein.

2.5. SUTRA-ICE equations

The SUTRA governing equations [27] modified for fully saturated soils, heat transport with ice formation are:

$$\left(S_w \rho S_{op} + \varepsilon \rho \frac{\partial S_w}{\partial p} \right) \frac{\partial p}{\partial t} + \left(\varepsilon (\rho_i - \rho) \frac{\partial S_i}{\partial T} + \varepsilon S_w \frac{\partial \rho}{\partial T} \right) \frac{\partial T}{\partial t} - \nabla \cdot \left[\left(\frac{k k_r \rho}{\mu} \right) \cdot (\nabla p - \rho g) \right] = Q_p \quad (13)$$

and

$$\begin{aligned} & \left[\varepsilon (S_w \rho c_w + S_i \rho_i c_i) + (1 - \varepsilon) \rho_s c_s - \varepsilon \rho_i L_f \frac{\partial S_i}{\partial T} \right] \frac{\partial T}{\partial t} \\ & + \varepsilon S_w \rho c_w \underline{v} \cdot \nabla T - \nabla \cdot \left\{ \left[\varepsilon S_w \left(\lambda_w \underline{I} + \underline{D} \right) + \varepsilon S_i \lambda_i \underline{I} + (1 - \varepsilon) \lambda_s \underline{I} \right] \cdot \nabla T \right\} \\ & = Q_p c_w (T^* - T) + \varepsilon S_w \rho \gamma_0^w + (1 - \varepsilon) \rho_s \gamma_0^s \end{aligned} \quad (14)$$

where S_{op} is the specified pressure storativity (the volume of water released from saturated pore storage due to a unit drop in fluid pressure per total solid matrix plus pore volume), p is pressure, t is time, \underline{k} is the permeability tensor, μ is the viscosity of liquid water, g is gravity, \underline{v} is the average fluid velocity, Q_p is porewater inflow, \underline{I} is the identity tensor, \underline{D} is the dispersion tensor, T^* is the temperature of the source fluid, and γ_0^w and γ_0^s are energy sources in the fluid and in the solid grains respectively. Eq. (13) describes the balance of water mass in variable density porewater as impacted by fluid fluxes due to temperature and pressure gradients, and Eq. (14) describes the balance of thermal energy as impacted by energy fluxes due to conduction, advection, and sources or sinks. The term $\varepsilon (\rho_i - \rho) \frac{\partial S_i}{\partial T}$ in Eq. (13) derives from application of Eq. (3). Eqs. (13) and (14) are the main governing equations and Eq. (6)–(12) describe the freezing functions and permeability during freezing in the SUTRA-ICE code. The equations as formulated do not include cryostatic pressure effects, which may draw liquid water towards the freezing zone [e.g. [39]].

2.6. Comparison with exact analytical solution

The SUTRA-ICE model is tested by comparison with the three-zone analytic solution presented by Lunardini [28]. This is an exact analytical solution for the propagation of subfreezing temperatures in a porous semi-infinite, initially nonfrozen medium with time, t . The solution is similar to the Neumann solution [40] for the movement of a freezing front that considers only two zones: a frozen and a thawed zone. The Lunardini solution divides the problem into three zones (Fig. 3) where zone 1 is fully frozen, with only the residual amount of unfrozen water; zone 2 is 'mushy', with both ice and water; and zone 3 is fully thawed. The Lunardini [28] solution is given below:

$$T_1 = (T_m - T_s) \frac{\text{erf}(x/2\sqrt{\alpha_1 t})}{\text{erf}(\psi)} + T_s \quad (15)$$

$$T_2 = (T_m - T_f) \frac{\text{erf}(x/2\sqrt{\alpha_4 t}) - \text{erf}(\gamma)}{\text{erf}(\gamma) - \text{erf}(\psi\sqrt{\alpha_1/\alpha_4})} + T_f \quad (16)$$

$$T_3 = (T_0 - T_f) \frac{-\text{erfc}(x/2\sqrt{\alpha_3 t})}{\text{erfc}(\gamma\sqrt{\alpha_4/\alpha_3})} + T_0 \quad (17)$$

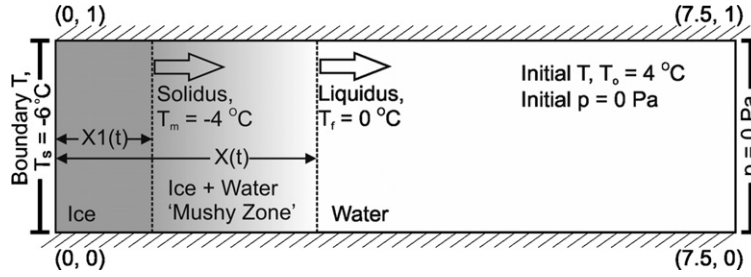


Fig. 3. Design of the simulation for comparing the SUTRA-ICE model with the Lunardini solution. $X_1(t)$ and $X(t)$, the distances from the specified temperature boundary to the solidus and liquidus respectively, increase with time, and can be calculated from the analytical Lunardini [28] solution (Eqs. (15)–(28)). Distances are in meters and the initial grid spacing is uniform with $\Delta x = 1$ cm and $\Delta y = 50$ cm.

where T_1 , T_2 , and T_3 are the temperatures at distance, x , from the temperature boundary for zones 1, 2, and 3, respectively; erf and erfc are the error function, and the complimentary error function respectively; T_0 , T_m , T_l , and T_s are the temperatures of the initial conditions; the solidus, the liquidus, and the boundary temperature, respectively; α_1 and α_3 are the thermal diffusivities for zones 1 and 3, respectively, defined as k_1/C_1 and k_3/C_3 where C_1 and C_3 are the volumetric bulk-heat capacities of the frozen and thawed zones, defined as:

$$C_1 = \varepsilon\rho_w c_w S_{wres} + \varepsilon\rho_i c_i (1 - S_{wres}) + (1 - \varepsilon)\rho_s c_s \quad (18)$$

$$C_3 = \varepsilon\rho_w c_w + (1 - \varepsilon)\rho_s c_s \quad (19)$$

and k_1 and k_3 are the bulk thermal conductivities of the frozen and thawed zones, defined as:

$$k_1 = \varepsilon\lambda_w S_{wres} + \varepsilon\lambda_i (1 - S_{wres}) + (1 - \varepsilon)\lambda_s \quad (20)$$

$$k_3 = \varepsilon\lambda_w + (1 - \varepsilon)\lambda_s \quad (21)$$

For the solution presented here, the thermal diffusivity of the mushy zone is assumed to be constant across the transition region, and the thermal diffusivity with latent heat term included, α_4 , is defined as:

$$\alpha_4 = \frac{k_2}{C_2 + \frac{\gamma_d L_f \Delta \xi}{(T_l - T_m)}} \quad (22)$$

where γ_d is the dry unit density of soil solids, $\gamma_d = (1 - \varepsilon)\rho_s$, and $\Delta \xi = \xi_0 - \xi_f$ where ξ_0 and ξ_f are the ratio of unfrozen water to soil solid mass for the fully thawed and frozen conditions, respectively, defined as:

$$\xi_0 = \frac{\varepsilon\rho_w}{(1 - \varepsilon)\rho_s} \quad (23)$$

$$\xi_f = \frac{\varepsilon S_{wres} \rho_w}{(1 - \varepsilon)\rho_s} \quad (24)$$

For a time, t , in the region from $0 \leq x \leq X_1(t)$ the temperature is T_1 (from Eq. (15)), where $X_1(t)$ is:

$$X_1(t) = 2\psi\sqrt{\alpha_1 t} \quad (25)$$

and from $X_1(t) \leq x \leq X(t)$ the temperature is T_2 (from Eq. (16)), where $X(t)$ is:

$$X(t) = 2\gamma\sqrt{\alpha_4 t} \quad (26)$$

and for $x \geq X(t)$ the temperature is T_3 (from Eq. (17)). The unknowns, ψ and γ , are found by iteratively solving the following two simultaneous equations:

$$\frac{(T_m - T_s)}{(T_m - T_l)} e^{-\psi^2(1-\alpha_1/\alpha_4)} = \frac{\frac{k_2}{k_1} \sqrt{\alpha_1/\alpha_4} \text{erf}(\psi)}{\text{erf}(\gamma) - \text{erf}(\psi\sqrt{\alpha_1/\alpha_4})} \quad (27)$$

$$\frac{(T_m - T_l)k_2/k_3}{T_0 - T_l} \sqrt{\alpha_3/\alpha_4} e^{-\gamma^2(1-\alpha_4/\alpha_3)} = \frac{\text{erf}(\gamma) - \text{erf}(\sqrt{\alpha_1/\alpha_4}\psi)}{\text{erfc}(\gamma\sqrt{\alpha_4/\alpha_3})} \quad (28)$$

Lunardini's [28] analytical solution assumes that the thermal diffusivity of the mushy zone is constant, and to allow direct comparison of values, the SUTRA-ICE code was modified to disallow the usual variability of this parameter for this particular situation. The choice of the relative permeability function for this case is arbitrary, as no flow occurs. Verification of the model against this analytical solution was attempted for the two sets of parameters given by Lunardini [41]: $T_m = -4$ °C and for $T_m = -1$ °C (Table 1). The SUTRA-ICE code results successfully match the analytical solution for these two sets of parameters (Fig. 4). The maximum absolute error for the $T_m = -4$ °C

Table 1
Parameters used in analytical solution by Lunardini [28]

Parameter	Value
T_0 (°C)	4
T_s (°C)	-6
T_l (°C)	0
T_m (°C) ^a	-4, -1
k_1 (J/s m C)	3.464352
k_2 (J/s m C)	2.941352
k_3 (J/s m C)	2.418352
C_1 (J/m ³ C)	690360
C_2 (J/m ³ C)	690360
C_3 (J/m ³ C)	690360
ξ_f (kg _{water} /kg _{solid})	0.0782
ξ_0 (kg _{water} /kg _{solid})	0.2
L_f (J/kg)	334720
γ_d (kg/m ³)	1680
γ^a	1.395, 2.062
ψ^a	0.0617, 0.1375

^a Model was run for two cases, $T_m = -4$ and $T_m = -1$.

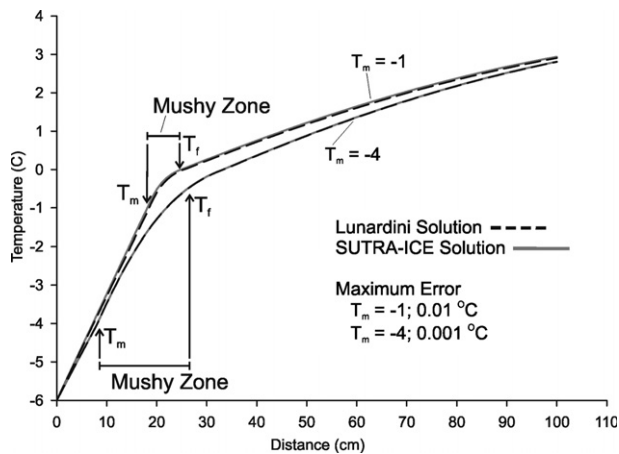


Fig. 4. Comparison of the results for the Lunardini solution to that of SUTRA-ICE, for $T_m = -4$ and $T_m = -1$.

case was $0.01\text{ }^\circ\text{C}$ or 0.1% of the total temperature range, and for the $T_m = -1\text{ }^\circ\text{C}$ case, the maximum absolute error was $0.1\text{ }^\circ\text{C}$ or 1% of the total temperature range. Thus, the SUTRA-ICE code properly represents the physics of soil freezing for a fully saturated porous medium with non-flowing water.

Table 2
Model parameters used in SUTRA-ICE simulations

Parameter	Lunardini	Frozen wall	Hill slope	Peat Bog
<i>Physical properties</i>				
Gravity (m/s^2)	0	0	-9.81	-9.81
Fluid specific heat (J/kg)	4187	4182	4182	4182
Ice specific heat (J/kg)	2108	2108	2108	2108
Ice thermal conductivity (J/s m C)	2.14	2.14	2.14	2.18
Density of ice (J/kg)	920	920	920	920
Latent heat of fusion (J/kg)	334000	334000	334000	334000
Fluid thermal conductivity (J/s m C)	0.58	0.6	0.6	0.58
Fluid compressibility [$\text{kg}/(\text{m s}^2)^{-1}$]	0	0	4.47×10^{-10}	0
Solid matrix compressibility [$\text{kg}/(\text{m s}^2)^{-1}$]	0	0	10^{-8}	0
Solid grain specific heat (J/kg)	840	840	840	1920
Solid grain conductivity (J/s m C)	2.9	3.5	3.5	.25
Density of solid grains (kg/m^3)	2600	2600	2600	1300
Porosity (-)	0.05	0.1	0.1	0.4
Permeability (m^2)	10^{-10}	10^{-10}	10^{-10}	10^{-10}
Anisotropy ($k_{\text{vertical}}: k_{\text{horizontal}}$)	1:1	1:1	1:100	1:1
Longitudinal dispersivity (m)	0	5	5	0.4
Transverse dispersivity (m)	0	0.5	1	0
<i>Time step controls</i>				
Time step size (h)	0.25	^a	6	1
Total simulation time (days)	1	800	365.25	390
<i>SUTRA-ICE parameters</i>				
Freezing function	L_{sw}	EXP	L_{sw}	EXP
Freezing function parameters	$m = 0.25\text{--}2.0$	$W = 0.5$	$m = 1$	$W = 0.05$
Residual saturation	0	0.05	0.025	0.005
Relative permeability method	L_{kr}	IMP	L_{kr}	IMP
Relative permeability parameters	N/A	$\Omega = 50$	N/A	$\Omega = 5$
Minimum K_r	10^{-6}	10^{-6}	10^{-6}	10^{-6}

EXP = Lunardini, Eq. (9); L_{sw} = linear saturation method, Eq. (6); L_{kr} = linear relative permeability method, Eq. (11); imp = impedance relative permeability method, Eq. (12).

^a Time step is variable: Initial time step = 1 h; Multiplier for time step change cycle = 2; Number of time steps in time step change cycle = 6; Maximum allowed time step size = 12 h.

2.7. Sensitivity of freezing process to freezing function shape

The sensitivity of the shape of the freezing function and the latent heat was evaluated by simulating a Neumann-type problem using the linear freezing function for four parameter sets, $m = 0.25, 0.5$, and 1.0 , and $m = 0.5$ without latent heat. The other parameters are the same as the Lunardini simulation (Table 2) and the results are shown in Fig. 5. Use of a steep freezing function results in a narrow freezing front having a small distance between the liquidus (i.e. the freezing point, $0\text{ }^\circ\text{C}$) and the solidus (i.e. the point at which the soil freezing function reaches the residual saturation). Using less-steep freezing functions results in a wider mushy zone. The difference in onset distances of freezing may be due to the large amount of latent heat released that hinders additional ice formation, and the amount of release is controlled by the slope of the freezing function.

Without latent heat, the temperature and saturation profiles are entirely controlled by heat capacities and thermal conductivities of the water and ice. The effect of latent heat is much greater than just the heat capacities, and as such it controls the distribution of temperature and ice. The release of latent heat acts to 'slow' progres-

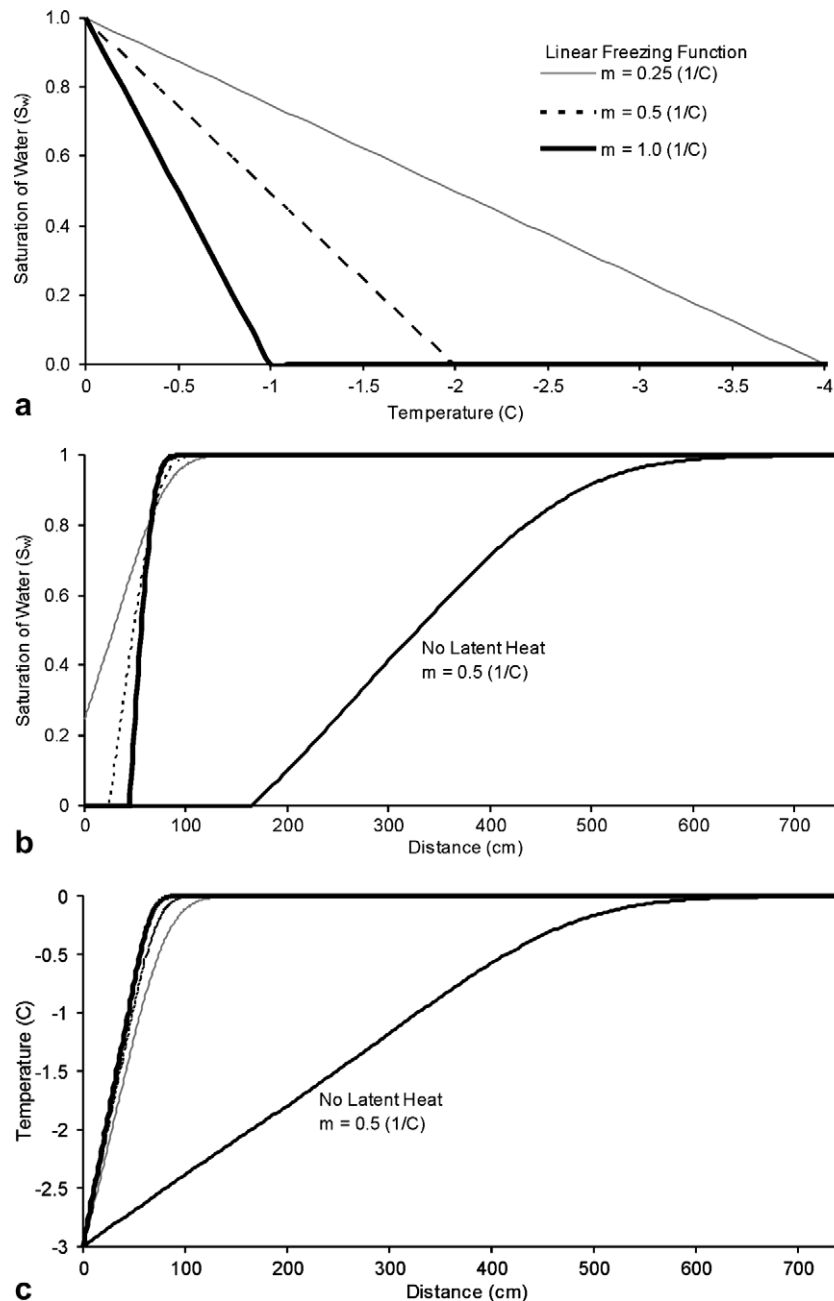


Fig. 5. Results from using three sets of parameters for the linear freezing function (a) with the model setup as show in Fig. 3. (b) and (c) show the results for the saturation and the temperature with distance respectively.

sion of the freezing front and to create a steeper temperature divide between the fully frozen and unfrozen regions.

3. Benchmarking suggestions

Models that incorporate both mass and energy transport with ice formation are difficult to verify against analytical solutions because there are few solutions that solve this problem. Solutions that are available [41,42] focus primarily on either ice-forming or melting with static water, are usually 1-dimensional. Following are two suggested heat

transport problems that may be used for comparison of model results among simulation codes that represent the freeze–thaw process.

3.1. Frozen wall problem

The “frozen wall problem” is a 2-dimensional areal model with warm porewater (5 °C) flowing into a domain that is partially intersected by a region with a specified sub-freezing temperature (−5 °C). The simulation is in the horizontal plane, thereby negating variable density flow. The parameters used in the problem are given in Table 2 and

the configuration and boundary conditions are described in Fig. 6. This configuration, although hypothetical, is chosen because it is similar to what is expected for frozen soil boundaries used in the remediation of groundwater contamination [43]. The modeled area is initially at a temperature of 5 °C and water of the same temperature steadily recharges the area from one side. At the start of the simulation, a specified subfreezing temperature is set within the hypothetical wall, which is held at this temperature throughout the simulation. This may be considered as one half-section of a larger region containing a series of walls with uniform spacing that are perpendicular to the regional groundwater flow direction.

The simulation results of the frozen wall problem are shown in Figs. 7 and 8. At the -5 °C specified temperature boundary region (i.e., the wall), ice forms along the leading edge of the boundary and a wedge of ice is formed behind the boundary. The cold temperatures from the ice boundary are conducted both upstream and downstream. The ice forms an essentially impermeable barrier to flow, forcing porewater to flow around the wall at a higher velocity due to the decreased flow area. The ice distribution reaches steady state conditions by 800 days. Fig. 8 compares results for the linear and exponential freezing functions. The linear freezing function does not decrease in value as quickly as the exponential function, thereby allowing more water flow through the mushy zone and creating a wider ice-forming zone and greater distribution of colder temperature water downgradient from the frozen wall. Numerical convergence experiments showed that the results of the simulation do not change appreciably for models with finer mesh-spacing or with shorter initial and maximum time step size.

3.2. Hill slope with seasonal freezing problem

The hill slope benchmark problem is a simplified cold region groundwater flow system, wherein recharge from a local topographic high discharges to two water bodies (e.g. lakes) with different surface elevations. During winter the topographic recharge system is ‘cut off’ by ground

freezing, and flow then is predominately from the higher lake to the lower lake (Fig. 9). The exchange of energy between the atmosphere and ground surface is represented in a simple manner using a thermal boundary layer. The air temperature is described by a sinusoidal function with a 10° amplitude centered on an average annual temperature of 2 °C with a period of 1 year:

$$T_{\text{air}} = 2 - \left[10 \sin \left(\frac{2\pi t}{365.25} \right) \right] \quad (29)$$

where t is the time in days, and T_{air} is the air temperature. The boundary layer is represented within the model as a 1 m thick porous medium, with a thermal conductivity of 1.25 W/m °C, essentially zero permeability ($k = 10^{-40}$ m²), and zero heat capacity. The boundary layer is modeled by specifying these thermal conductivity and permeability values for the top row of elements, with heat capacities in the top row of nodes set to zero. In the row of nodes just below the thermal boundary layer is a specified-pressure boundary condition, with a pressure of zero representing conditions at the water table. Any water that flows into the hillside from the specified pressure boundary has the same temperature as the air (Eq. (29)). The point of this combination of the boundary layer and water recharge is to accommodate two thermal conditions at the land surface. During recharge, the subsurface thermal regime is mainly impacted by the temperature of recharging water and during the cold no-recharge period, when ice blocks the pores, the air temperature is conducted to the ground through the boundary layer.

The bottom of the model has a no-flow boundary condition and a specified temperature boundary condition of 2 °C. This approximates the conditions at a confining unit below which groundwater remains at 2 °C throughout the year. The pressure along the bottom of the lakes is the hydrostatic pressure of the water column, set in the model as a depth-dependent specified hydrostatic pressure. The parameters used in the hillside problem are given in Table 2 and the configuration and boundary conditions are described in Fig. 9. The simulation was run for a total of one year using a 6 h time step.

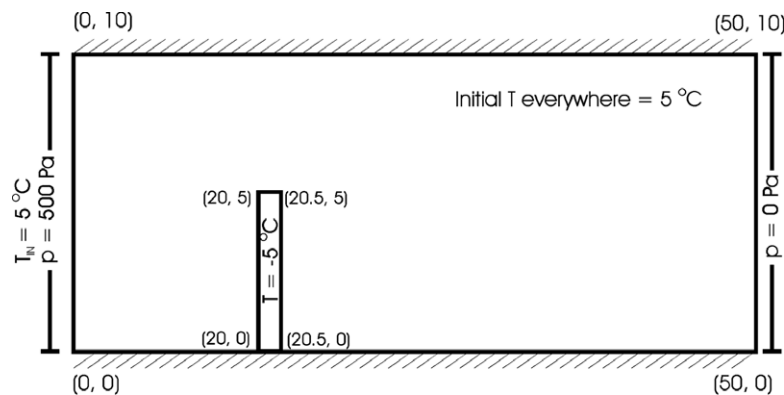


Fig. 6. Design of suggested frozen wall benchmark problem. The grid spacing was $\Delta x = \Delta y = 0.5$ m. T_{IN} is the temperature of inflowing fluid. Distances are in meters and (x, y) locations refer to (horizontal, vertical) distances.

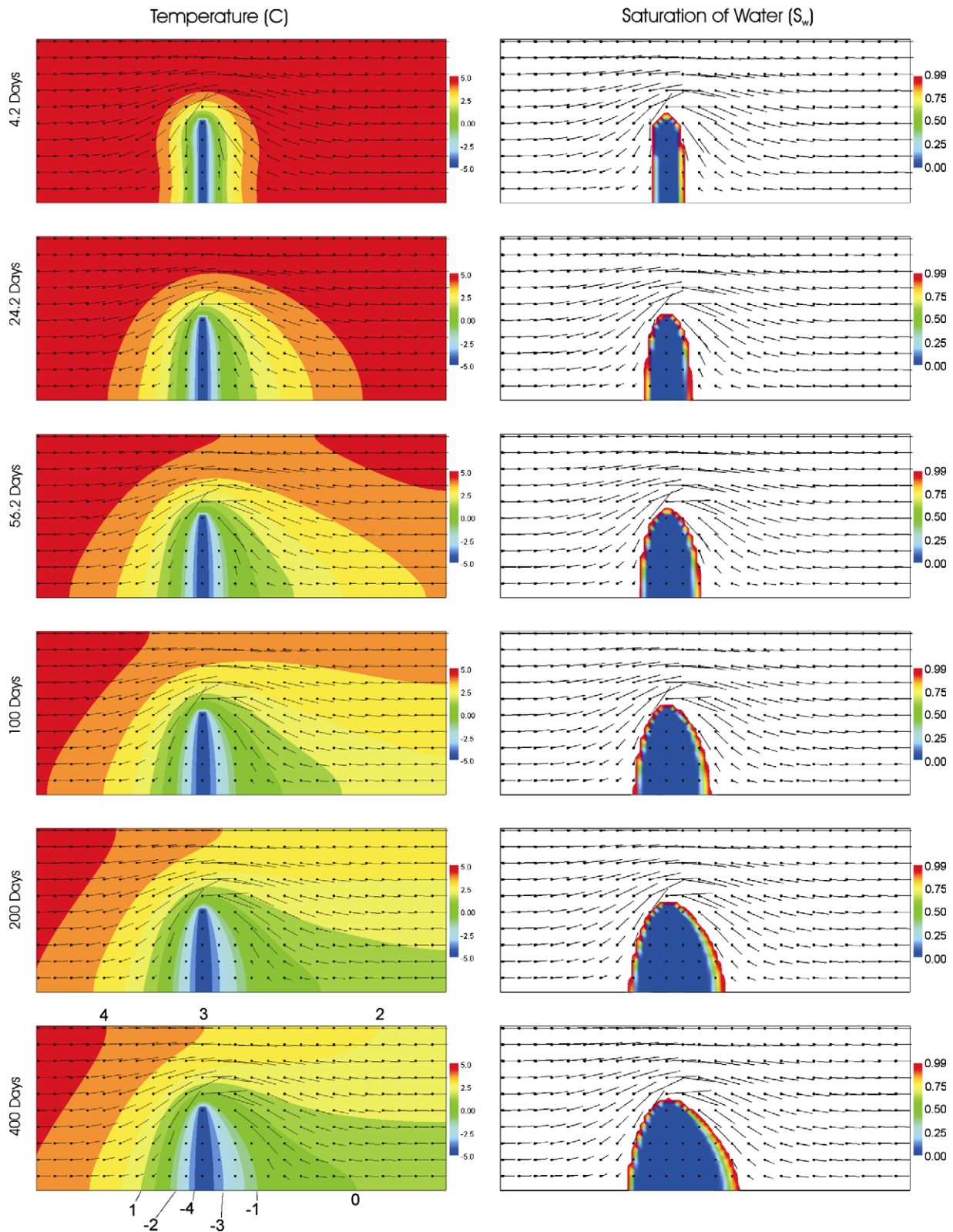


Fig. 7. Temperature, ice saturation and velocity results for the frozen wall benchmark problem at various time increments. The steady state results (800 days) are in Fig. 8. The results are with the exponential freezing function ($\nu = 0.025$; residual = 0.025) and the impedance relative permeability function ($\Omega = 10$). For the saturation of water (S_w) results, the white area has a saturation of 1. The velocity vectors move away from the square vector base.

A mesh and time-step refinement study was used to ensure that the presented solution does not depend on mesh-spacing and time-step size. The zone in which ice

forms requires very small vertical grid spacing ($\Delta y \leq 6$ cm), but the model results do not vary significantly for time step sizes less than 24 h. Models that have higher frequency

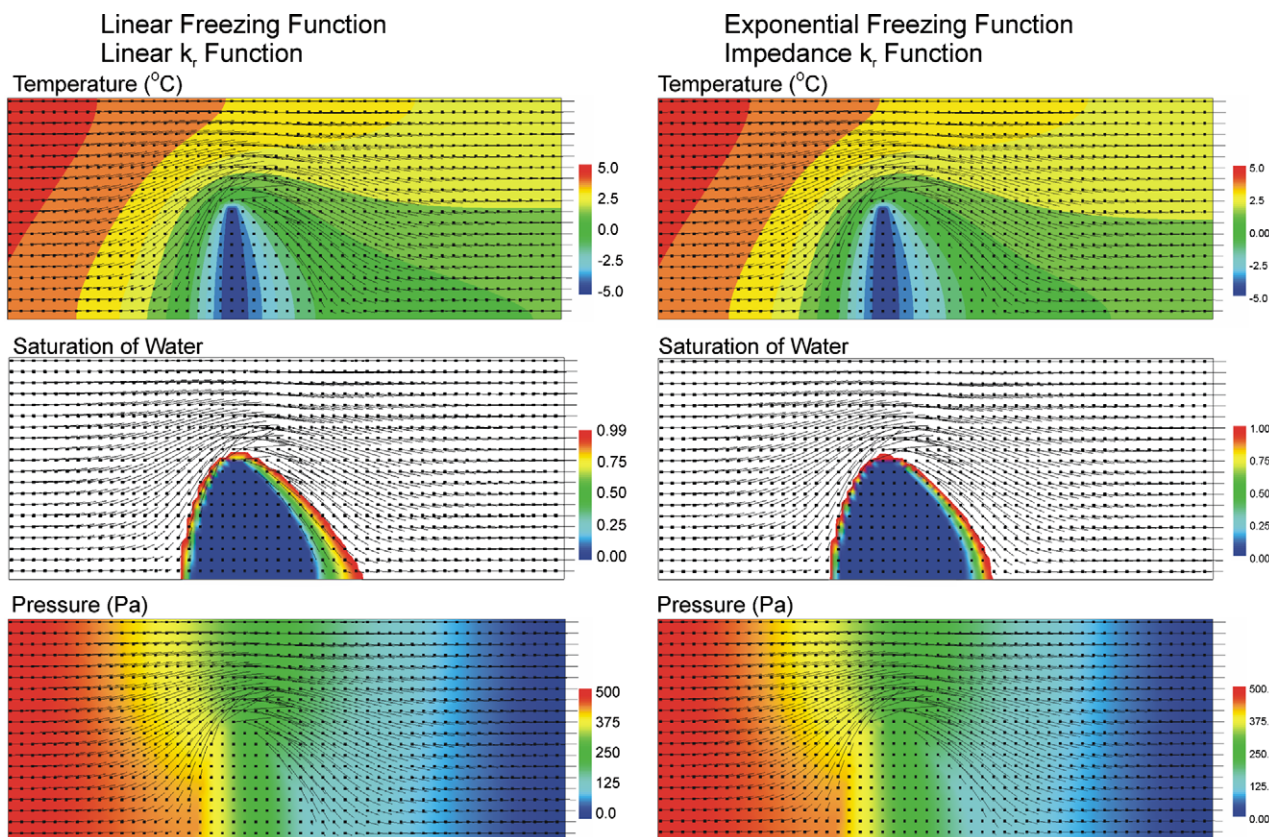


Fig. 8. Comparison of the results of wall freezing problem at 800 days (steady state) for the linear freezing and permeability functions versus the exponential freezing function and the impedance relative permeability function. For the saturation of water results, the white area has a saturation of 1. The velocity vectors indicate flow away the square base, and the magnitude is proportional to the length of the line.

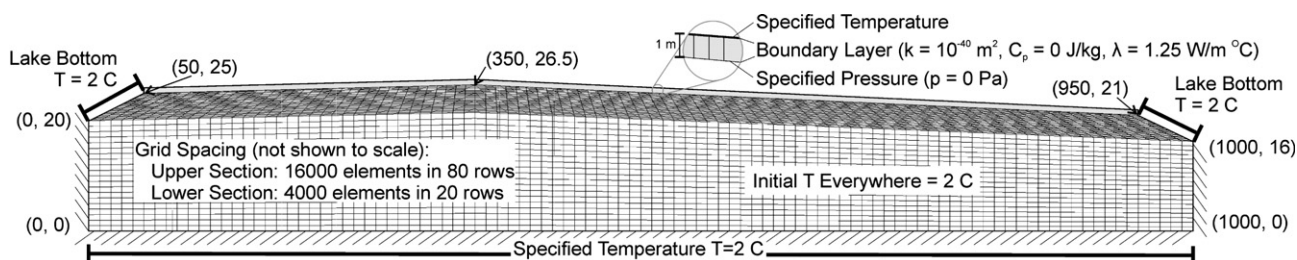


Fig. 9. Design of a suggested 2-dimensional hill-slope benchmark problem. The top 2 rows of nodes, from $x = 50$ to 950 m, simulate a boundary layer as described in the text. The boundary layer is a 1 m thick row of elements with a row of specified-temperature nodes for the surface temperature and row of specified-pressure nodes for the land surface. The sloped upper right and upper left corners of the model represent lakes. The lake bottoms, represented by specified-pressure nodes, are set to hydrostatic pressure of the lake water column and any water that flows into the aquifer from a lake has a temperature of 2 degC. Distances are in meters and (x, y) locations refer to (horizontal, vertical) distances.

temperature boundary fluctuations may require a smaller time-step.

The simulated ground surface temperatures are shown in Fig. 10, the temperature and ice saturation results are shown in Fig. 11 and detailed temperature and saturation results below the hill crest are in Table 3. Results show that there is a several-degree difference in air- and ground surface temperature (at the specified pressure boundary) during parts of winter and summer seasons due to the simulated thermal boundary layer, including a lag in ground surface warming in the spring. As temperatures

at the ground surface decrease below freezing, subsurface ice starts to form first at the hillcrest, because cold water is most strongly advected downwards in this region. As the subzero temperatures propagate into the near-surface layers of the model, the relative permeability decreases, cutting off the downward vertical flow, and separating the zone of active groundwater recharge into two parts that shift downhill towards each lakes. When winter-time hilltop recharge is essentially stopped, the flow field is then predominately from the higher lake to the lower lake.

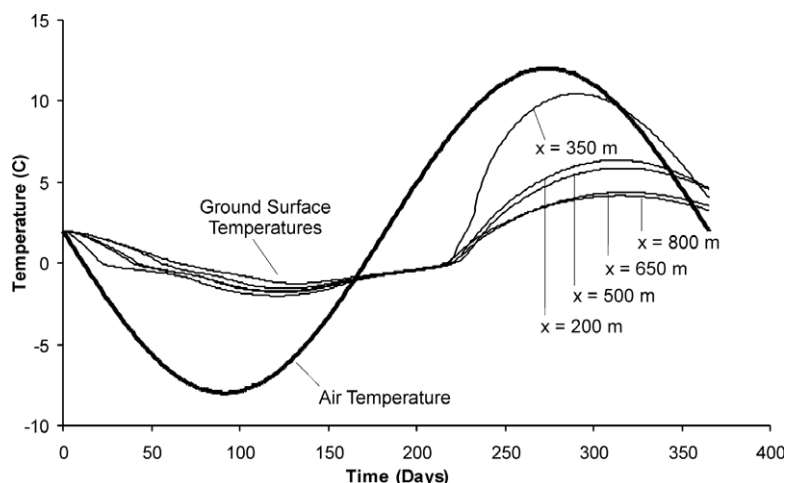


Fig. 10. Temperatures across the boundary layer in the hill-slope model. Ground surface temperatures and air temperatures refer to temperatures at the specified pressure and specified temperature boundaries respectively. The x distances refer to horizontal distance from the left edge of the model in meters.

During the spring, when the surface temperatures rise above freezing, the ice first vanishes nearest the lakes and this open zone progressively extends up the hill slopes, while at the same time the ice zone melts from above. Above the melting ice zone, a very shallow flow system connects the hillcrest and the larger flow systems via water flowing above the remnant ice zone. During the summer the original flow system is restored, and warm water is advected into the model, in particular at the hillcrest of the model where the porewater flow direction is primarily downward. At the end of the first-year cycle, a warm region of water remains underground that affects ice formation the following year (by preferentially warming the region below the hillcrest). It takes several years to reach a dynamic steady state wherein the ice evolution for each yearly cycle is the same (not shown).

4. Freezing in a peat bog

The field temperature data used to test the modified numerical model was obtained from an intensively instrumented bog in the Glacial Lake Agassiz Peatlands, Minnesota [44,45] (Fig. 12). At the crest of a large raised bog, thermocouples were installed at 0, 25, 50, 75, 100, 125, 150, 200, 250, 300, 350, and 400 cm depths [6]. Temperature and atmospheric pressure were measured approximately 1 m above the land surface. The data are stored with a solar powered data logger connected to a mobile phone for data access. From June 18, 1998, to August 18, 2000, temperature data were averaged at a minimum of every 5 min and a maximum of an hour per day (Fig. 12; shows first 14 months only). The hydraulic head data were averaged over 5 min to 1 h intervals [46].

The instrumentation was installed at the hydrologic divide on the crest of the Red Lake Bog where porewater mostly moves in the vertical plane [46]. Here, because of dimensionality considerations [47], moving heat and water can be simulated as vertical, 1-dimensional flow.

There are cyclical seasonal and daily changes in the temperature profiles in the peat. The main control on the thermal cycles is temperature at the surface of the peat profile (Fig. 12). The temperature at the base of the peat profile is nearly constant at $\sim 4.8^\circ\text{C}$. The surface peat temperature fluctuates from -34.1 to 25.9°C over the course of the data-collection period, and the pattern of fluctuations is a subdued replica of the local air temperature.

To model the temperature profiles at the site with SUTRA-ICE, a specified pressure condition ($p = 0$ Pa) for the top boundary, reflecting the water table was used and no-flow boundaries were used on the sides. The elevation of the groundwater table was held constant at the peat surface because the elevation of the water table only fluctuated a small amount (<10 cm) over the period of record. The bottom of the model was a specified temperature boundary.

The energy transport model was run in transient mode with 2 h time steps. Specified-temperature boundaries were applied to the top and bottom of the model. The input temperature values for the heat boundaries were changed daily based on mean daily temperature values taken from the field measurements of air temperature at the peat surface and water temperature at the bottom of the peat column.

An important calibration variable was the shape of the freezing function, with a steeper function decreasing the ice zone's extent. The freezing curve used in calibrating the model was based on the wide range of values for peat that were compiled by Farouki [14]. The porosity was also an important variable in calibrating the energy transport model. The calibrated model had a high effective porosity of 40%, which was realistic considering that peat has very high water content. The porosity affects the energy transport primarily in winter; as ice forms, latent heat is released and the bulk thermal conductivity of the system changes as the ratio of water to ice changes.

The SUTRA-ICE simulation closely represents both the depth of ice and the measured temperature profiles at the

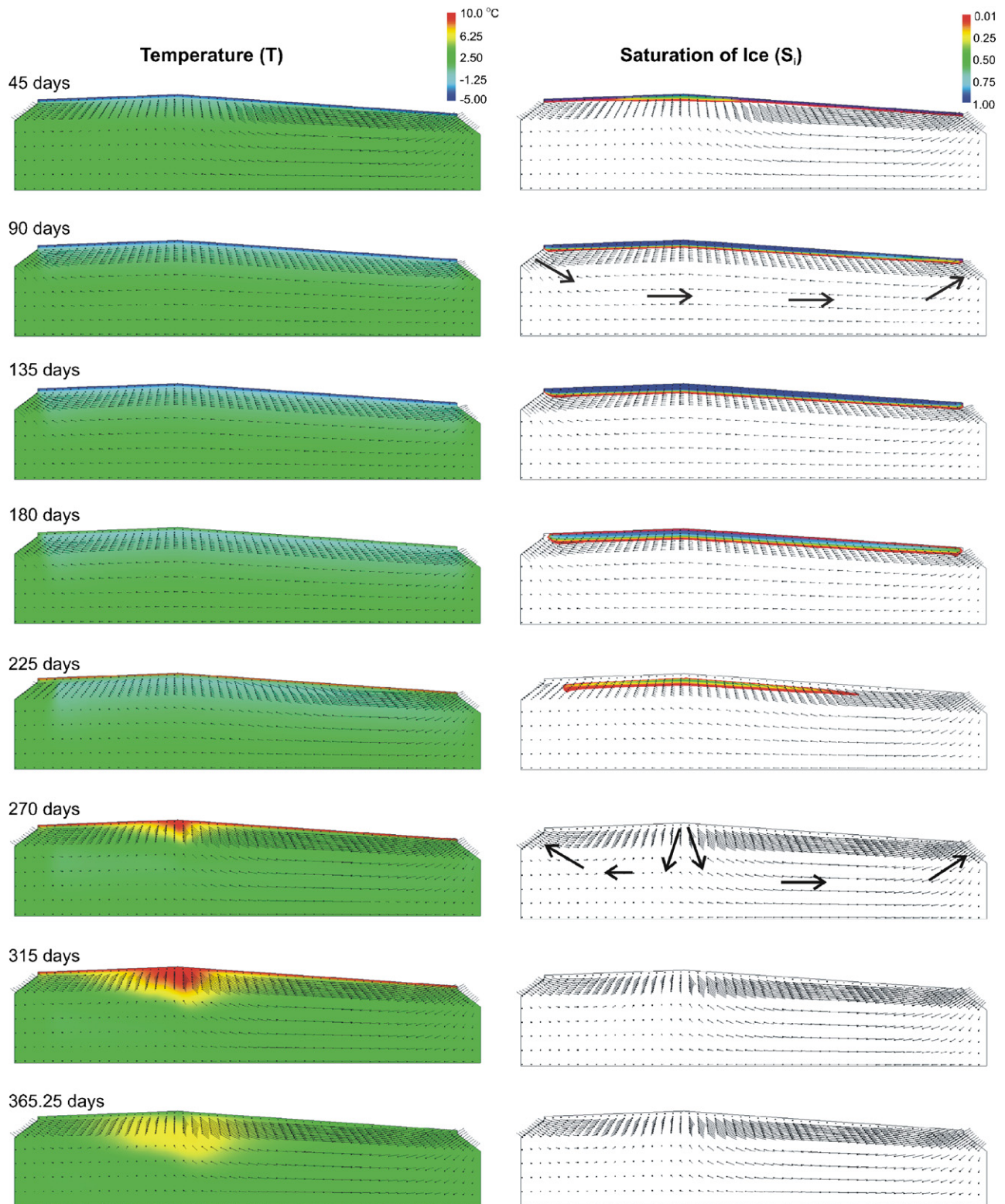


Fig. 11. Results of the hill-slope model for temperature, saturation, and velocity. The velocity vectors indicate flow away the square base, and the magnitude is proportional to the length of the line. The ice saturation indicates the percentage of pore-space filled by ice; ice saturation less than 1% is not shaded. The 90 and 270 day saturation results have illustrative arrows showing the generalized winter and summer flow regime respectively.

Red Lake Bog, MN (Fig. 13). The measured and modeled results both show that the $0\text{ }^{\circ}\text{C}$ isotherm did not penetrate below 25 cm depth during the winters of 1999 and 2000,

indicating that the SUTRA-ICE code was able to suitably simulate the depth of ice formation. In addition to matching the temperature profiles well, the SUTRA-ICE model

Table 3
Detailed near-surface temperature and ice saturation results for the hill slope problem at the hill-crest ($x = 350$)

Time ^b	Depth ^a																						
	-100		0		50		100		150		200		250		300		350		400		450		500
	Air T	T^c	S_i^d	T	S_i	T	S_i	T	S_i	T	S_i	T	S_i	T	S_i								
0	2.00	2.00	0.00	2.00	0.00	2.00	0.00	2.00	0.00	2.00	0.00	2.00	0.00	2.00	0.00	2.00	0.00	2.00	0.00	2.00	0.00	2.00	0.00
25	-2.17	-0.12	0.06	0.03	0.00	0.21	0.00	0.39	0.00	0.59	0.00	0.79	0.00	0.97	0.00	1.14	0.00	1.29	0.00	1.42	0.00	1.54	0.00
50	-5.58	-0.51	0.63	-0.21	0.15	-0.04	0.01	0.08	0.00	0.19	0.00	0.31	0.00	0.43	0.00	0.55	0.00	0.67	0.00	0.79	0.00	0.90	0.00
75	-7.61	-1.08	0.98	-0.31	0.32	-0.07	0.02	0.05	0.00	0.16	0.00	0.28	0.00	0.38	0.00	0.49	0.00	0.59	0.00	0.69	0.00	0.79	0.00
100	-7.89	-1.81	0.99	-0.78	0.91	-0.16	0.10	-0.01	0.00	0.10	0.00	0.20	0.00	0.31	0.00	0.41	0.00	0.50	0.00	0.59	0.00	0.69	0.00
125	-6.37	-1.99	0.99	-1.16	0.99	-0.40	0.47	-0.09	0.03	0.02	0.00	0.12	0.00	0.22	0.00	0.32	0.00	0.41	0.00	0.50	0.00	0.58	0.00
150	-3.32	-1.58	0.99	-1.11	0.99	-0.59	0.74	-0.17	0.11	-0.03	0.00	0.06	0.00	0.15	0.00	0.24	0.00	0.33	0.00	0.41	0.00	0.50	0.00
175	0.69	-0.85	0.94	-0.79	0.91	-0.56	0.71	-0.24	0.20	-0.07	0.02	0.02	0.00	0.10	0.00	0.19	0.00	0.27	0.00	0.35	0.00	0.42	0.00
200	4.94	-0.45	0.55	-0.59	0.75	-0.48	0.60	-0.25	0.23	-0.09	0.03	-0.01	0.00	0.07	0.00	0.15	0.00	0.22	0.00	0.30	0.00	0.37	0.00
225	8.66	1.37	0.00	0.16	0.00	-0.40	0.47	-0.25	0.22	-0.11	0.05	-0.03	0.00	0.05	0.00	0.12	0.00	0.18	0.00	0.25	0.00	0.32	0.00
250	11.16	7.73	0.00	7.28	0.00	6.71	0.00	6.10	0.00	5.48	0.00	4.86	0.00	4.26	0.00	3.68	0.00	3.15	0.00	2.66	0.00	2.23	0.00
275	12.00	10.08	0.00	9.81	0.00	9.45	0.00	9.04	0.00	8.60	0.00	8.13	0.00	7.64	0.00	7.14	0.00	6.62	0.00	6.10	0.00	5.59	0.00
300	11.01	10.32	0.00	10.21	0.00	10.04	0.00	9.84	0.00	9.60	0.00	9.33	0.00	9.03	0.00	8.69	0.00	8.33	0.00	7.95	0.00	7.55	0.00
325	8.38	8.86	0.00	8.90	0.00	8.92	0.00	8.93	0.00	8.90	0.00	8.84	0.00	8.75	0.00	8.63	0.00	8.48	0.00	8.29	0.00	8.08	0.00
350	4.59	6.12	0.00	6.29	0.00	6.49	0.00	6.68	0.00	6.86	0.00	7.00	0.00	7.13	0.00	7.22	0.00	7.28	0.00	7.30	0.00	7.29	0.00
365.25	2.00	4.05	0.00	4.30	0.00	4.59	0.00	4.88	0.00	5.15	0.00	5.41	0.00	5.65	0.00	5.86	0.00	6.04	0.00	6.19	0.00	6.30	0.00

^a Depth, in cm, is the depth below the simulated land surface. At the hill crest, 0 cm depth is at $y = 26.5$ m.

^b Time is in days.

^c T is temperature in °C.

^d S_i is the saturation of ice- the fraction of pore space filled by ice. An S_i of 0 indicates there is no ice.

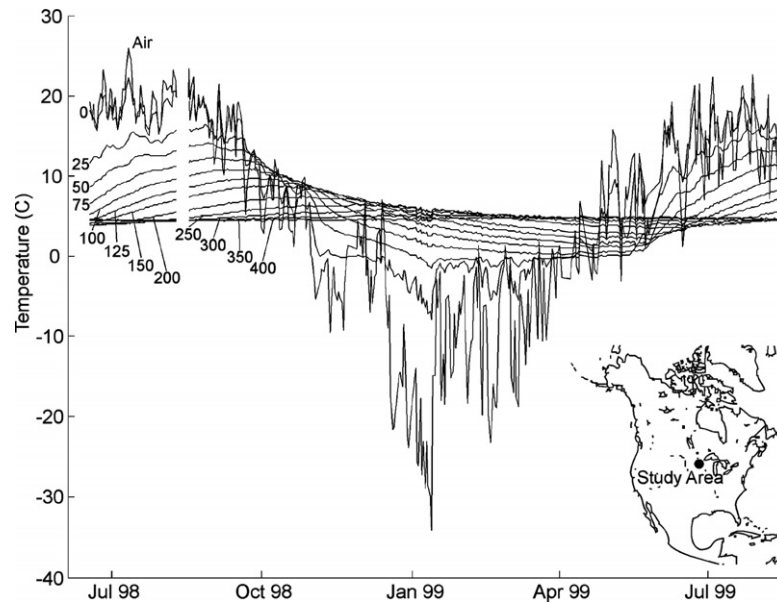


Fig. 12. The measured temperature data, which were simulated using the modified SUTRA model, from the crest of the Red Lake Bog, Glacial Lake Agassiz Peatland, Minnesota. The data gap was a result of field instrumentation failure. The inset shows the location of the field site.

was able to correctly predict the timing of the rise in temperature in the spring due to melting of ice. For comparison, the same model was run without the ice routine (i.e. using the standard SUTRA code; [6]), and for the latter simulation, spring temperatures warm too soon. This confirms that ice formation and melting is a process that must be considered when evaluating the thermal regime in cold climates.

5. Conclusions

In northern peatlands the formation and melting of near-surface ice is an important process in the control of heat transport and microbial activity [6]. The ice-formation process in soils is analogous to desaturation processes in the unsaturated zone, with ice-forming over a range of a range of subfreezing temperatures until only the residual water content remains. During the phase transition latent heat is released, a process that can be modeled using an apparent heat capacity. An existing groundwater flow and energy transport code (SUTRA) was enhanced to include these freeze/thaw processes.

SUTRA-ICE, a new model built on the existing SUTRA framework, can simulate the formation and melting of ice. The model was successfully verified by comparing its results to an analytical solution and by matching field data. Further verifications or improvements will ideally occur by other researchers comparing their ice-forming model with the benchmark problems offered herein, or by suggesting additional benchmarks.

The shape of the freezing function is found to be very important in controlling the rate and extent of ice formation. The simplified freezing functions used in the SUTRA-ICE code capture the primary impacts of freezing

on large hydrologic behavior. However, within the code, users can easily implement other or more complicated freezing functions. As ice forms over a range of temperatures, latent heat is released in proportion to the slope of the freezing function. If more ice is formed over a shorter temperature interval, then more latent heat will be released over a smaller temperature range. The released latent heat has a higher energy content than the heat capacities of ice and water, and during freezing, it significantly slows further growth of ice [15].

Two possible benchmark problems are suggested that may be used for comparison of other groundwater and energy transport codes that incorporate subsurface freezing and thawing. The first problem is an areal model with a frozen barrier deflecting porewater flow. The second problem is a hill slope cross section with yearly sinusoidally-varying air temperature inducing the formation of a freezing zone that decreases and eventually ends groundwater recharge to the hill, before melting during spring thaw. The two suggested benchmark problems also show the potential impact that ground ice may have on subsurface hydrology.

A simulation considering both freezing and thawing is necessary to explain the time changes in the vertical temperature profiles in a peat bog in northern Minnesota. The SUTRA-ICE model successfully matched both the temperature distribution within the peat profile and the timing of ice thaw in the spring.

The model applied here assumes, as a first approximation, that the thermal properties of ice are constant for all temperatures, whereas thermal conductivity and heat capacity of ice actually change with decreasing temperature. Furthermore, the current version of the SUTRA-ICE model does not represent freezing in the unsaturated

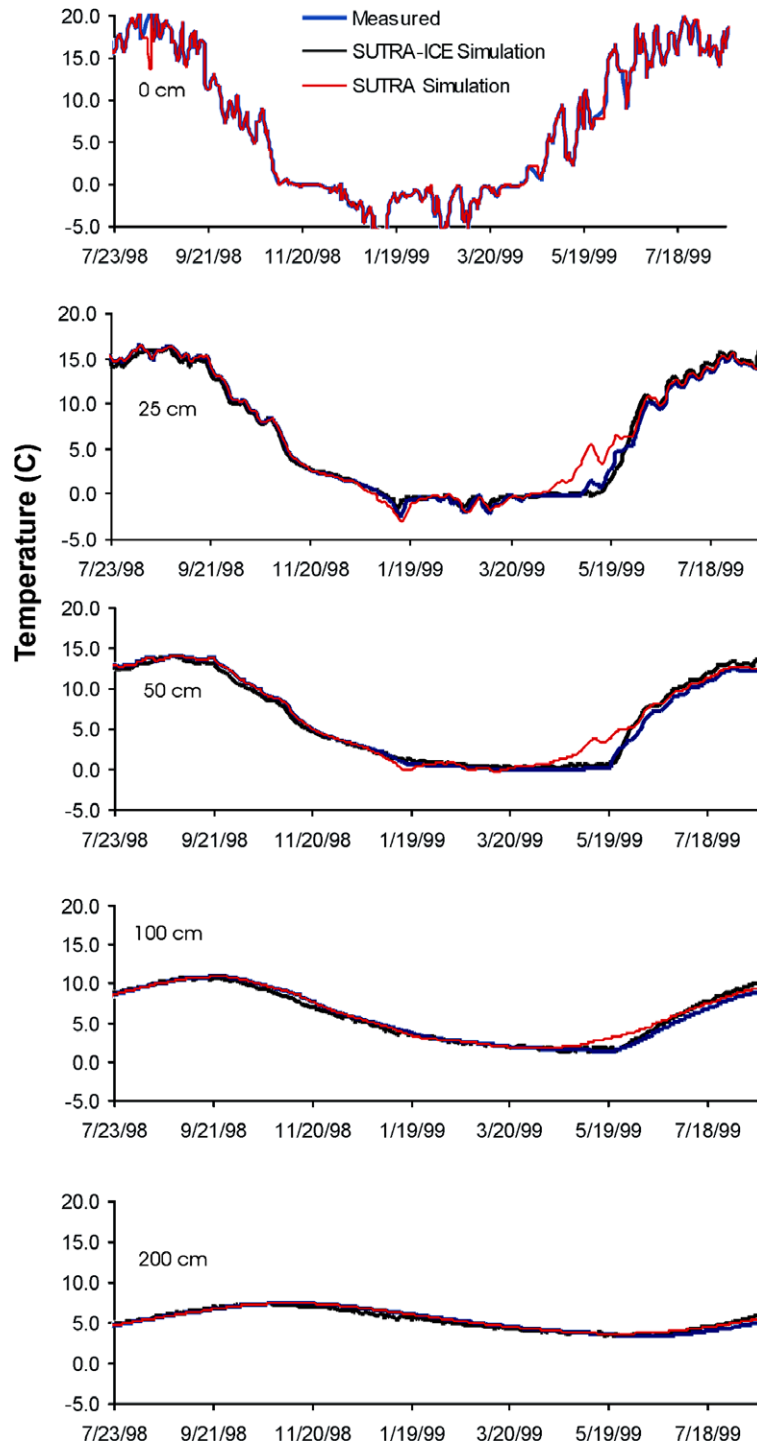


Fig. 13. Comparison of measured results for the Red Lake Bog temperature profiles with that of SUTRA and SUTRA-ICE. The two simulations were run with identical parameters. Profiles are shown at the following depths: 0 cm, 25 cm, 50 cm, 100 cm, and 200 cm.

zone or solute transport and the impact of solutes on freezing. If the k_r and S_w functions do not monotonically decrease with decreasing temperatures below freezing, then spurious porewater velocity may be present with ice formation. It is not clear whether these results are realistic and so here, it is assumed that with the formation of ice in pores, the porewater velocity will decrease, constraining the selec-

tion of functionality for relative permeability and ice saturation.

A code such as the SUTRA-ICE model can be used for a variety of cold climate applications. Northern peatlands are a major source of atmospheric methane, and the role of ice formation affects the extent and timing of heat transport into the peat profile. The model can also be used to

study the impact of near-surface ice formation on regional hydrogeology, groundwater recharge, and contaminant transport. In addition, the 2-dimensional and 3-dimensional SUTRA-ICE model may be used as a standard groundwater flow model that includes the interaction of subsurface ice with regional groundwater flow patterns.

Acknowledgements

This paper would not be possible without the generous help of Paul Glaser and Donald Rosenberry in data collection. We also thank Helen French, Laura Lautz, and other anonymous reviewers for their comments.

References

- [1] Cary JW, Mayland HF. Salt and water movement in unsaturated frozen soil. *Soil Sci Soc Am Proc* 1972;36:549–55.
- [2] Fuchs M, Campbell GS, Pependick RI. An analysis of sensible and latent heat flow in a partially unsaturated soil. *Soil Sci Soc Am J* 1978;42:379–85.
- [3] Harlan RL. Analysis of coupled heat-fluid transport in partially frozen soil. *Water Res Res* 1973;9:1314–23.
- [4] Serreze MC, Walsh JE, Chapin III FS, Osterkamp T, Dyrgerov M, Romanovsky V, et al. Observational evidence of recent change in the northern high-latitude environment. *Climatic Change* 2000;46:159–207.
- [5] Smith LC, Sheng Y, MacDonald GM, Hinzman LD. Disappearing arctic lakes. *Science* 2005;308:1429.
- [6] McKenzie JM, Siegel DI, Rosenberry DO, Glaser PH, Voss CI. Heat transport in the Red Lake Bog, Glacial Lake Agassiz Peatlands. *Hydrol Proc*, in press, doi:10.1002/hyp6239.
- [7] Hunt RJ, Krabbenhoft DP, Anderson MP. Groundwater inflow measurements in wetland systems. *Water Res Res* 1996;32:495–507.
- [8] Woo M-K, Marsh P. Snow, frozen soils and permafrost hydrology in Canada, 1999–2002. *Hydrol Process* 2005;19:215–29.
- [9] Romanovsky VE, Osterkamp TE. Effects of unfrozen water on heat and mass transport processes in the active layer and permafrost. *Permafrost Periglac* 2000;11:219–39.
- [10] Kane DL, Hinkel KM, Goering DJ, Hinzman LD, Outcalt SI. Non-conductive heat transfer associated with frozen soils. *Global Planet Change* 2001;29:275–92.
- [11] Grant SA, Iskandar IK. Contaminant hydrology : cold regions modeling. Boca Raton: Lewis Publishers; 2000.
- [12] Narasimhan TN. Fourier's heat conduction equation; history, influence, and connections. *Rev Geophys* 1999;37:151–72.
- [13] Deming D, Sass JH, Lachenbruch AH, De Rito RF. Heat flow and subsurface temperature as evidence for basin-scale ground-water flow, North Slope of Alaska. *Geol Soc Am Bull* 1992;104:528–42.
- [14] Farouki O. Thermal properties of soils. Clausthal-Zellerfeld Germany: Trans Tech, 1986.
- [15] Williams PJ, Smith MW. The frozen earth; fundamentals of geocryology. Cambridge, UK: Cambridge University Press; 1989.
- [16] Lundin L-C. Hydraulic properties in an operational model of frozen soil. *J Hydrol* 1990;118:289–310.
- [17] Hwang CT, Murray DW, Brooker EW. A thermal analysis for structures on permafrost. *Canad Geotech J* 1972;9:33–46.
- [18] Hansson K, Simunek J, Mizoguchi M, Lundin L-C, Genuchten MTv. Water flow and heat transport in frozen soil. *Nume Sol Freeze-Thaw Appl Vadose Zone J* 2004;3:693–704.
- [19] Simunek J, Sejna M, van Genuchten MT. The HYDRUS-1D software package for simulating the one-dimensional movement of water, heat, and multiple solutes in variably-saturated media; Version 2.0, U.S. Salinity Laboratory, U.S. Department of Agriculture, 1998.
- [20] Ippisch O. Coupled transport in natural porous media. Combined faculties for the natural sciences and for mathematics. Heidelberg, Germany: Rupertus Carola University; 2001. p. 123.
- [21] Mottaghy D, Rath V. Implementation of permafrost development in a finite difference heat transport code. 2005.
- [22] Clauser C. SHEMAT: A simulator for mass and heat transport. Springer; 2003.
- [23] White MD, Oostrom M. STOMP; Subsurface transport over multiple phases; Version 2.0; Theory Guide, Pacific Northwest National Laboratory, 2000.
- [24] Jansson P-E, Karlberg L. Coupled heat and mass transfer model for soil-plant-atmosphere systems. Stockholm: Royal Institute of Technology, Department of Civil and Environmental Engineering; 2004.
- [25] Flerchinger GN. The simultaneous heat and water (SHAW) Model: Technical Documentation; Technical Report NWRC 2000-09. Boise, Idaho: Northwest Watershed Research Center; USDA Agricultural Research Service, 2000.
- [26] Krahn J. Thermal modeling with TEMP/W; an engineering methodology. Calgary, Canada: GEO-SLOPE International, Ltd.; 2004.
- [27] Voss CI, Provost AM. SUTRA; A model for saturated-unsaturated, variable-density ground-water flow with solute or energy transport, Water-Resources Investigations Report 02-4231, 2002.
- [28] Lunardini VJ. Freezing of soil with phase change occurring over a finite temperature difference. Proceedings of the 4th international offshore mechanics and arctic engineering symposium. ASM; 1985.
- [29] Voss CI. A finite-element simulation model for saturated-unsaturated, fluid-density-dependent ground-water flow with energy transport or chemically-reactive single-species solute transport. Water-Resources Investigations Report 84-4369, U.S. Dept. of the Interior Geological Survey ;, 1984.
- [30] Goodrich LE. An introductory review of numerical methods for ground thermal regime calculations; 1061, National Research Council of Canada Division of Building Research, 1982.
- [31] Lunardini VJ. Freezing of soil with an unfrozen water content and variable thermal properties. Hanover, NH: U.S. Army Corps of Engineers Cold Regions Research and Engineering Laboratory; 1988.
- [32] Jame Y-W, Norum DI. Heat and mass transfer in a freezing unsaturated porous medium. *Water Res Res* 1980;16:811–9.
- [33] Bittelli M, Flury M, Campbell GS. A thermoelectric analyzer to measure the freezing and moisture characteristic of porous media. *Water Res Res* 2003;39. doi:10.1029/2001WR000930.
- [34] Koopmans RWR, Miller RD. Soil freezing and soil water characteristic curves. *Proc Soil Sci Soc Am* 1966;30:680–5.
- [35] Spaans EJA, Baker JM. The soil freezing characteristic: its measurement and similarity to the soil moisture characteristic. *Soil Sci Soc Am J* 1996;60:13–9.
- [36] Black PB. Applications of the Clapeyron equation to water and ice in porous media. Hanover, NH: U.S. Army Corps of Engineers Cold Regions Research and Engineering Laboratory; 1995.
- [37] Grant SA. Physical and chemical factors affecting contaminant hydrology in cold environments. ERDC/CRREL TR-00-21. Hanover, NH: U.S. Army Corps of Engineers Engineer Research and Development Center; 2000.
- [38] van Genuchten MT. A closed-form equation for predicting the hydraulic conductivity of unsaturated soils. *Soil Sci Soc Am J* 1980;44:892–8.
- [39] Fowler AC, Krantz WB. A generalized secondary frost heave model. *SIAM J Appl Math* 1994;54:1650–75.
- [40] Carslaw HS, Jaeger JC. Conduction of heat in solids; 2nd Ed., 2d. Oxford, Clarendon Press, 1959.
- [41] Lunardini VJ. Heat transfer with freezing and thawing. Amsterdam, NY: Elsevier; 1991.
- [42] Lunardini VJ. Heat transfer in cold climates. New York: Van Nostrand Reinhold Company; 1981.
- [43] Andersland OB, Wiggert DC, Davies SH. Frozen soil subsurface barriers; formation and ice erosion. *J Contam Hydrol* 1996;23:133–47.

- [44] Glaser PH, Chanton JP, Morin PJ, Rosenberry DO, Siegel DI, Ruud O, et al. Surface deformation as indicators of deep ebullition fluxes in a large northern peatland. *Global Biogeochem Cycles* 2004;18. doi:10.1029/2003GB002069.
- [45] Siegel DI, Reeve AS, Glaser PH, Romanowicz EA. Climate-driven flushing of pore water in peatlands. *Nature* 1995;374: 531–3.
- [46] Rosenberry DO, Glaser PH, Siegel DI, Weeks EP. Use of hydraulic head to estimate volumetric gas content and ebullition flux in northern peatlands. *Water Res Res* 2003;39. doi:10.1029/2002WR001377.
- [47] Anderson MP, Woessner WW. *Applied groundwater modeling: simulation of flow and advective transport*. San Diego, CA: Academic Press; 1992.